Interior Structure and Seasonal Mass Redistribution of Mars from Radio Tracking of Mars Pathfinder

W. M. Folkner,* C. F. Yoder, D. N. Yuan, E. M. Standish, R. A. Preston

Doppler and range measurements to the Mars Pathfinder lander made using its radio communications system have been combined with similar measurements from the Viking landers to estimate improved values of the precession of Mars' pole of rotation and the variation in Mars' rotation rate. The observed precession of –7576 ± 35 milliarc seconds of angle per year implies a dense core and constrains possible models of interior composition. The estimated annual variation in rotation is in good agreement with a model of seasonal mass exchange of carbon dioxide between the atmosphere and ice caps.

Little is known about the interior of Mars. From telescopic observations and spacecraft missions, the mass and radius of Mars have been determined and hence its mean density. Because Mars is significantly asymmetric, its polar moment of inertia C cannot be inferred from the gravity field. Determination of the polar moment of inertia yields information on the distribution of mass within the planet, such as whether the planet has a dense core surrounded by a lighter mantle. Analysis of radio tracking measurements from the Viking landers has determined the normalized polar moment of inertia C/MR^2, where M is the mass of Mars and R is its mean radius, to be 0.355 ± 0.015 (*1*). However, the uncertainty in this estimate is not small enough to determine with certainty that Mars has a dense core or to distinguish between interior models ranging from an Earth-like composition to iron-enriched compositions characteristic of the meteorites thought to originate from Mars (*2*).

The Mars Pathfinder mission has provided an opportunity to improve our knowledge of Mars' polar moment of inertia and hence our knowledge of Mars' interior. As with the Viking landers, the Pathfinder radio system used for communication with Earth was also used to measure the distance (from the signal travel time) and changes in distance (from the Doppler frequency shift of the signal) between Earth and Mars. These measurements provided information on the changing orbits of Earth and Mars and on the rotation of Mars (*3*). Of particular interest is the martian rotational information: secular precession and periodic nutation of the spin axis, seasonal and tidal variations in the rotation rate, and Chandler-like wobble of Mars' figure axis relative to the spin axis. These quantities can be used to constrain models of the interior of Mars and estimate the annual mass exchange between the atmosphere and the polar ice caps.

The precession is driven by the gravitational torque of the sun acting on Mars' oblate figure and is proportional to $(C - (A + B)/2)/C$ where $C > B > A$ are the principal moments of inertia of Mars. The factor $C - (A + B)/2 = J_2MR^2$ is already known with high accuracy from detection of Mars' gravity field with the use of Viking orbiter and other tracking data (*4*). Accurate measurement of the precession is needed to determine the polar moment of inertia. Knowledge of the moment of inertia, combined with measurements of Mars' mass, size, shape, and low-order gravity harmonics, provides key information for models of the interior structure.

In addition to providing insight into the interior of Mars, the polar moment of inertia is of interest in determining the martian climate over millions of years. Due to the action of the sun, Jupiter, and other planets, the obliquity of Mars varies by tens of degrees (*5*). The change in obliquity causes large changes in insolation that result in dramatic changes in climate (*6*). The history of the obliquity depends on the value of the moment of inertia, and a more precise determination of the moment of inertia provides better estimates of the history of insolation.

Mars' rotation rate is expected to vary because of redistribution of mass by seasonal sublimation and condensation of carbon dioxide at the polar ice caps (*7*). Smaller variations are expected as a result of gravitational solar tides. The size of the variations depends on the amount of mass redistribution and on the internal structure.

The Pathfinder tracking data acquired from landing on 4 July 1997 through the end of September 1997 have been used in combination with tracking data from the Viking landers to determine improved estimates of the precession and seasonal rotation variations of Mars. The combined data set is powerful, in spite of the relatively short span of the Pathfinder data, because of the large movement of the martian pole from precession between the time of the Viking lander mission and the Pathfinder mission. The Viking lander data give the mean spatial orientation of the pole of rotation of Mars at the midpoint of that experiment, whereas the Pathfinder data give the pole orientation about 20 years later. In addition, improved estimates of the seasonal variations in rotation rate, compared to previous Viking results, have been achieved by including 2 years of Doppler data from the Viking I lander (recovered by R. Wimberly) that were not included in previous analyses. The Pathfinder data span is too short to significantly improve estimates of seasonal variations in rotation rate.

Because the Pathfinder radio system operates at a higher frequency than the Viking lander radio systems, the Doppler data are much less affected by fluctuating charged particles in the solar system and in Earth's ionosphere (*8*). The Pathfinder ranging measurements are similarly more accurate than the Viking lander measurements, partly because of the higher communications frequency and partly because of improvements in ground station calibrations.

The Pathfinder and Viking lander tracking measurements have been analyzed to solve for Mars rotation and orbit parameters. The rotation from Mars-fixed coordi-

Table 1. Estimated Mars rotation constants. Numbers in parentheses indicate uncertainties in the final digit or digits.

Parameter	Value
Obliquity ε (degrees)	25.189417 (35)
Obliquity rate $d\varepsilon/dt$ (mas/year)	1 (16)
Node ψ (degrees)	35.43777 (14)
Precession rate $d\psi/dt$ (mas/year)	−7576 (35)
Rotation about pole ϕ (degrees)	133.61259 (fixed)
Rotation rate $d\phi/dt$ (degrees/day)	350.89198521 (8)
Annual term $C1$ (mas)	504 (57)
Annual term $S1$ (mas)	−170 (81)
Semiannual term $C2$ (mas)	−107 (56)
Semiannual term $S2$ (mas)	−82 (59)
Triannual term $C3$ (mas)	−25 (61)
Triannual term $S3$ (mas)	−12 (53)
Quarterly term $C4$ (mas)	−41 (38)
Quarterly term $S4$ (mas)	31 (40)

Jet Propulsion Laboratory, California Institute of Technology, 4800 Oak Grove Drive, Pasadena, CA 91109, USA.

*To whom correspondence should be addressed. E-mail: william.folkner@jpl.nasa.gov

nates to inertial coordinates was modeled by rotation about the spin axis and nutation and precession of the spin axis. Rotation about the spin axis was described by angle ϕ, its rate ω, and harmonics

$$\delta\phi = \sum_{j=1}^{4} \{C_j \cos j\ell + S_j \sin j\ell\}$$

where ℓ is the orbital mean anomaly (*9*). The angle ϕ at the epoch J2000 was held fixed and defined the longitude system. The rate of rotation ω was estimated. The nutation model was adopted from Reasenberg and King (*10*). Mars' obliquity ε (the angle between the equatorial and orbital plane) and its rate $d\varepsilon/dt$ were estimated, as were the longitude of the node (of intersection between the orbital and equatorial planes) ψ and the precession rate $d\psi/dt$ (*11*). Also estimated were three coordinates for each lander, six parameters describing Mars' orbit, and three parameters (equivalent to the semimajor axis, eccentricity, and longitude of perihelion) describing the shape of Earth's orbit. The orientation of Earth's orbit with respect to the frame of extragalactic radio sources used to define Earth orientation was held fixed (*12*).

Table 1 gives the estimated rotation constants. The uncertainties indicated in Table 1 are five times the standard deviations. The factor of 5 accounts for the failure to account for various systematic effects, including polar motion, and encompasses variations in solutions observed with subsets of the data and solution parameters. The estimated obliquity rate is consistent with zero, as expected. The precession rate is inversely proportional to the normalized polar moment of inertia C/MR^2, as given by (*13*)

$$d\psi/dt = -\frac{3}{2} J_2 \cos\varepsilon (1 - e^2)^{-3/2} MR^2 n^2/\omega C$$

where e is the orbital eccentricity. The corresponding moment estimate is

$$C/MR^2 = 0.3662 \pm 0.0017$$

For purposes of cartography, it is standard to decompose the rotation of Mars as a rotation about the spin axis, with the spin axis direction described by its right ascension α and declination δ (*14*). For convenience, Table 2 gives the estimated cartographic constants for Mars based on the Pathfinder and Viking data. Because most cartographers will not account for nutation, this model does not account for nutation (*15*). Table 3 gives cylindrical lander coordinates consistent with this rotation model. Cylindrical coordinates are most natural for the data analysis, because the longitude and distance from the spin axis are determined well by short data arcs, whereas the determination of the distance from the equator requires a longer data arc and is more correlated with estimated orbital parameters. Geodetic lander coordinates are given in Table 4 for cartographic purposes.

Previous estimates of Mars' polar moment of inertia required assumptions about the source of triaxial asymmetry of the internal mass distribution. Reasenberg (*16*) used the observed triaxial shape of Mars and the hypothesis that the Tharsis volcano was the primary contribution to the nonhydrostatic component of the polar moment to estimate a value for C/MR^2 of 0.365. One means of understanding Reasenberg's argument is to consider the relative magnitude of the nonhydrostatic contributions to the three moments of inertia $\Delta C \geq \Delta B \geq \Delta A$. Tharsis is located near the equator and is aligned with the A moment axis. Reasenberg effectively argued that $\Delta C = \Delta B$. On the other hand, Bills (*17*) argued that the most likely case is $\Delta C - \Delta B = \Delta B - \Delta A$. The expected moment from this argument is $C/MR^2 = 0.345$. Our estimate favors the Reasenberg interpretation.

The estimated polar moment of inertia can be used to constrain models of the martian interior (*1*, *18*). The polar moment of inertia varies with core size, composition, and temperature profile. We consider models with mantle compositions ranging from an Earth-like molar ratio of Mg/(Mg+Fe), χ_M, of 89% to a value of 70%, representing a mantle highly enriched with iron; and two possible temperature profiles, one cooler than Earth at a given pressure and one warmer (Fig. 1). The estimated precession constant rules out most of the models. Warm models with mantle compositions similar to that of Earth (for example, χ_M = 89%) are ruled out, as are some cold iron-rich models ($\chi_M < 70\%$). However, the core radius can range from 1200 to 2400 km without an additional constraint such as core composition. The core has been modeled as an Fe-FeS mixture. For each suite of models, the smallest core radius corresponds to a nearly pure iron core (except for the models with χ_M = 70%), whereas the largest core radius is with an FeS core. The composition of meteorites thought to have originated on Mars favors a martian mantle

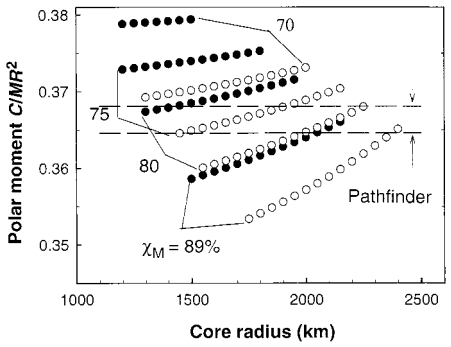

Fig. 1. Polar moment of inertia versus core radius for four different mantle compositions and two different temperature profiles. The solid circles indicate models with temperatures 200 K lower than Earth at the same pressure; the open circles indicate models with temperatures 200 K higher than Earth (*1*).

Table 2. Estimated cartographic constants for Mars. Numbers in parentheses indicate uncertainties in the final digit or digits.

Parameter	Value
Pole right ascension at J2000 α (degrees)	317.68143 (1)
Right ascension rate $d\alpha/dt$ (degrees/century)	−0.1061 (7)
Pole declination at J2000 δ (degrees)	52.88650 (3)
Declination rate $d\delta/dt$ (degrees/century)	−0.0609 (4)
Rotation about pole at J2000 W (degrees)	176.901 (fixed)
Rotation rate ω (degrees/day)	350.89198226 (8)

Table 3. Cylindrical lander coordinates. Numbers in parentheses indicate uncertainties in the final digit or digits.

	Pathfinder	Viking 1 lander	Viking 2 lander
Longitude (degrees)	W33.5238 (1)	W48.2217 (5)	E134.0100 (6)
Distance from spin axis (km)	3203.206 (1)	3136.519 (1)	2277.386 (6)
Height above equator (km)	1108.89 (9)	1284.41 (5)	2500.01 (5)

Table 4. Geodetic lander coordinates with respect to a reference ellipsoid defined by an equatorial radius of 3397.2 km and flatness 0.0105. Numbers in parentheses indicate uncertainties in the final digit or digits.

	Pathfinder	Viking 1 lander	Viking 2 lander
Longitude (degrees)	W33.5238 (1)	W48.2217 (5)	E134.0100 (6)
Latitude (degrees)	19.4724 (14)	22.6969 (7)	48.2688 (5)
Height from ellipsoid (km)	−3.61 (3)	−2.69 (2)	4.23 (4)

composition with χ_M near 75%. In this case, and if the core composition satisfies FeS/(Fe + FeS), $\chi_S < 50\%$, then the core radius must be in the range of 1450 to 1700 km for warm models. The moment constraint for cold models with $\chi_S < 50$ tends to favor mantle compositions with χ_M near 80% and core radii in the range of 1300 to 1450 km. In either case, Mars' core is a considerably smaller fraction of the total planetary mass than is Earth's.

Variations in rotation about the spin axis are thought to be dominated by mass exchange between the polar caps and the atmosphere. During winter, part of the atmosphere condenses at the poles. If the southern cap increased symmetrically as the northern cap decreased, then there would not be any change in moment of inertia or rotation rate. However, because of Mars' orbital eccentricity, difference in elevation, and difference in albedo, the pole caps are not formed symmetrically. The unbalanced waxing and waning of the Martian polar ice caps results in seasonal changes in air pressure at the Pathfinder and Viking lander sites (*19*). If Mars has a liquid core, the change in rotation rate will depend on changes in the mantle polar moment of inertia C_m (assumed here to include the crust). Seasonal zonal winds, which are the primary mechanism for momentum change on Earth (*20*), are apparently much less important for Mars. Assuming that the north and south polar ice caps have uniform thickness and similar angular extent, the predicted change in rotation rate can be inferred from the pressure history (*1*, *21*)

$$\begin{aligned}\delta\phi(\text{mas}) = {} & 477\sin(\ell + 112.8°) \\ & + 204\sin(2\ell + 181.7°) \\ & + 25\sin(3\ell + 172.5°) \\ & + 10\sin(4\ell + 168.1°)\end{aligned}$$

A secondary source of rotation variations is the deformation of Mars' figure by solar tides. The predicted response is given by (*1*)

$$\delta\phi(\text{mas}) = -k_{2m}MR^2/C_m \begin{bmatrix} 97\sin(\ell) + 62\sin(2\ell + 2\omega_p - 2\psi) \\ + 14\sin(3\ell + 2\omega_p - 2\psi) + 7\sin(2\ell) \\ - 5.9\sin(2\ell + 2\omega_p - 2\psi) \end{bmatrix}$$

where k_{2m} is the mantle tidal Love number and ω_p is the longitude of periapsis measured from the intersection of the martian orbit and the ecliptic. The factor $k_{2m}MR^2/C_m$ ranges from 0.3 to 0.8 for plausible Mars models, with 0.5 taken as a nominal value.

The estimated annual term is in reasonably good agreement with the model (Fig. 2). The statistically significant shift from the previous result is thought to be due to systematic effects in the ranging data that were used exclusively in the previous analysis (*1*), whereas our seasonal estimates are dominated by the Viking Doppler data. The estimated semiannual term does not agree as well with the model (Fig. 3). This may indicate the needs for improvement in the model, improvements in the treatment of the data, or an unmodeled effect, such as interaction of the surface with winds. The estimated triannual and quarterly amplitudes are in fair agreement with the model but are not statistically significant (*22*).

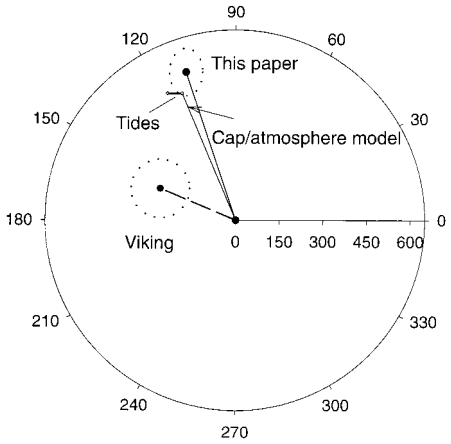

Fig. 2. Comparison of the amplitude and phase of the estimated annual variation in rotation with the model based on ice cap sublimation and accretion and solar tides. The phase is with respect to $\ell = 0°$. The estimate labeled "Viking" is taken from (*1*).

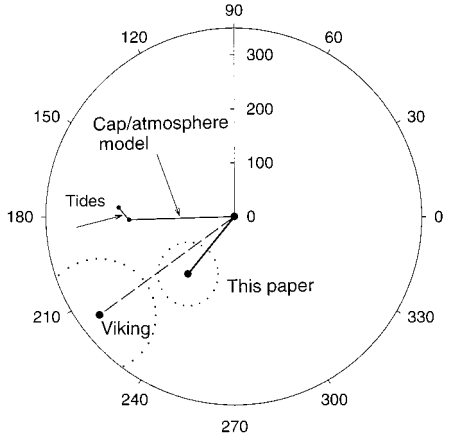

Fig. 3. Comparison of the amplitude and phase of the estimated semiannual variation in rotation with the model based on ice cap sublimation and accretion and solar tides. The phase is with respect to $\ell = 0°$. The estimate labeled "Viking" is taken from (*1*).

REFERENCES AND NOTES

1. C. F. Yoder and E. M. Standish, *J. Geophys. Res.* **102**, 4065 (1997).
2. For example, H. Y. McSween, *Meteoritics* **25**, 757 (1994); J. C. Laul, *Geochim. Cosmochim. Acta* **50**, 875 (1986).
3. W. M. Folkner *et al.*, *J. Geophys. Res.* **102**, 4057 (1997).
4. A. S. Konopliv and W. L. Sjogren, Publication 95–3, Jet Propulsion Laboratory, California Institute of Technology (1995); D. E. Smith *et al.*, *J. Geophys. Res.* **98**, 20871 (1995).
5. W. R. Ward, *J. Geophys. Res.* **79**, 3375 (1974); J. Touma and J. Wisdom, *Science* **259**, 1294 (1993).
6. For example, L. M. Francois, J. C. G. Walker, W. R. Kuhn, *J. Geophys. Res.* **95**, 14761 (1990).
7. A. Cazenave and G. Balmino, *Geophys. Res. Lett.* **8**, 245 (1981); B. F. Chao and D. P. Rubincam, *J. Geophys. Res.* **95**, 14755 (1990).
8. The Pathfinder radio system operates at X band (8 GHz) compared with the S-band (2 GHz) radio system used by the Viking landers. The Doppler data noise caused by solar plasma is inversely proportional to the square of the radio frequency. The Pathfinder Doppler data have about 13 times less noise than the Viking lander Doppler data. The Doppler data noise is about 0.05 mm/s for data at 60-s intervals. The solar plasma also affects the round-trip range measurements. Calibrations for the solar plasma for some of the Viking lander data were determined from dual-frequency observations of the Viking orbiters. The Viking ranging data have a residual noise of ~7 m for data with orbiter calibrations and ~12 m for data with no orbiter calibrations. The Pathfinder ranging data taken so far have residuals of ~3 m. The Pathfinder data analyzed here will be included in the mission data archive, to be available early in 1998 from the Planetary Data System.
9. The estimated terms on variation in rotation about the pole have been corrected for general relativistic effects. The relativistic correction results from the eccentric Mars orbit and orbital velocity, which alters local Mars time by a factor
$$\left(1 - GM_0/c^2r - \frac{1}{2}v^2\right)$$
See (*1*) and F. W. Sears and R. W. Brehme, *Introduction to the Theory of Relativity* (Addison-Wesley, Reading, MA, 1968).
10. R. D. Reasenberg and R. W. King, *J. Geophys. Res.* **82**, 369 (1977).
11. The obliquity at J2000 was determined with respect to the mean martian orbit of 1980. The mean orbit normal is described by $\alpha_o = 273.379°$ and $\delta_o = 65.323°$. The node is measured with respect to the intersection of the martian mean orbit and the Earth mean orbit of J2000.
12. W. M. Folkner *et al.*, *Astron. Astrophys.* **287**, 279 (1994).
13. Before computing *C*, a correction due to geodetic precession should be added to the observed precession. The nominal value is 6.7 milli–arc seconds (mas) per year [from (*10*)]. The normalized $J_2 = 0.001.9586$ (*4*), the orbital eccentricity $e = 0.09341$, and the effective mean motion $n = 191.408°$ per year.
14. For example, M. E. Davies *et al.*, *Celest. Mech.* **63**, 127 (1996).
15. To compare with Table 1, the precession rate is obtained from $d\psi/dt = -|d\mathbf{z}/dt \times \mathbf{z}|^2/(\sin^2\varepsilon)$, where $\mathbf{z} = \mathbf{n}_p \times \mathbf{n}_o$ defines the line of nodal intersection, $\mathbf{n}_p$ is the normal to the equator, and $\mathbf{n}_o$ is the normal to the orbit. The explicit expression is $d\psi/dt = 1.0305\, d\alpha/dt + 1.6136\, d\delta/dt$. The unmodeled nutations shift this estimate by about –100 mas/year. The rotation rate dW/dt differs from ω because the rotations about the pole α and δ are not eigen directions for the precession, which thus affects dW/dt.
16. R. D. Reasenberg, *J. Geophys. Res.* **82**, 369 (1977); W. M. Kaula, *Geophys. Res. Lett.* **6**, 194 (1979).
17. B. Bills, *Geophys. Res. Lett.* **16**, 385 (1989).
18. F. Sohl and T. Spohn, *J. Geophys. Res.* **102**, 1613 (1997).
19. J. E. Tillman, N. C. Johnson, P. Guttorp, D. B. Percival, *ibid.* **98**, 10963 (1993).
20. R. D. Rosen and D. A. Salstein, *ibid.* **88**, 5451 (1983).
21. The model in (*1*) depends on cap size and ice mass distribution. The values quoted here assume uniform caps that extend to 65° latitude and sublimate and accrete uniformly over their surfaces.
22. The predicted triannual amplitude from air pressure and tides is $20\sin(\ell + 180°)$ mas and is reasonably